

Temporal Perceiver: A General Architecture for Arbitrary Boundary Detection

Jing Tan Yuhong Wang Gangshan Wu Limin Wang \boxtimes

State Key Laboratory for Novel Software Technology, Nanjing University, China

{jtan, yhwang24}@smail.nju.edu.cn, {gswu, lmwang}@nju.edu.cn

Abstract

*Generic Boundary Detection (GBD) aims at locating general boundaries that divide videos into semantically coherent and taxonomy-free units, and could serve as an important pre-processing step for long-form video understanding. Previous research separately handle these different-level generic boundaries with specific designs of complicated deep networks from simple CNN to LSTM. Instead, in this paper, our objective is to develop a general yet simple architecture for arbitrary boundary detection in videos. To this end, we present **Temporal Perceiver**, a general architecture with Transformers, offering a unified solution to the detection of arbitrary generic boundaries. The core design is to introduce a small set of latent feature queries as anchors to compress the redundant input into fixed dimension via cross-attention blocks. Thanks to this fixed number of latent units, it reduces the quadratic complexity of attention operation to a linear form of input frames. Specifically, to leverage the coherence structure of videos, we construct two types of latent feature queries: boundary queries and context queries, which handle the semantic incoherence and coherence regions accordingly. Moreover, to guide the learning of latent feature queries, we propose an alignment loss on cross-attention to explicitly encourage the boundary queries to attend on the top possible boundaries. Finally, we present a sparse detection head on the compressed representations and directly output the final boundary detection results without any post-processing module. We test our Temporal Perceiver on a variety of detection benchmarks, ranging from shot-level, event-level, to scene-level GBD. Our method surpasses the previous state-of-the-art methods on all benchmarks, demonstrating the generalization ability of our temporal perceiver.*

1. Introduction

Video content analysis [5, 23, 37, 40, 41, 45] is an important problem in computer vision on account of the drastic growth in videos that are uploaded and shared on the Inter-

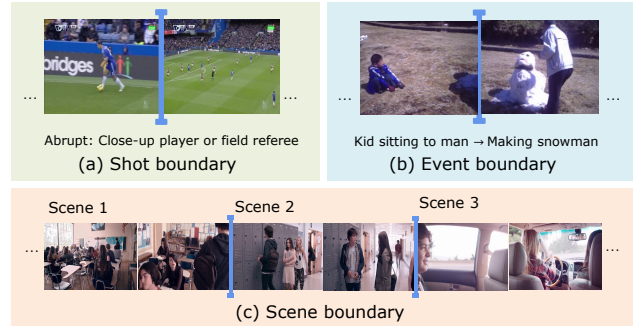


Figure 1. Examples of generic boundaries, from shot-level, event-level to scene-level boundary.

net. Long-form video understanding is still under-explored in previous literature. We study the problem of arbitrary generic boundary detection, which can serve as an advantageous technique to bridge the gap between long-form and short-form video understanding, by segmenting long videos into a series of shorter videos [34]. Different from the well-studied action instance boundaries [2, 16, 24, 43, 44], generic boundaries are naturally emerge due to semantic incoherence and not specific to any pre-defined semantic category. Figure 1 provides examples of generic boundaries from shot-level, event-level to scene-level instances. To detect such diverse generic temporal boundaries, different level information is expected for capturing temporal structure and context at different scales.

Current research on generic boundary detection is divided into several different tasks based on their own boundary semantics and granularity. Camera shot segmentation [10] targets at shot-level boundaries (Figure 1a) that are rapid transitions between camera shots. Generic event boundary detection (GEBD) [34] aims to locate event-level generic boundaries (Figure 1b) which are moments where the action/subject/environment changes. Scene segmentation [20] tries to detect scene-level generic boundaries (Figure 1c), which are transits between movie scenes, marking the twists of the high-level plot. However, the target videos of these tasks share the same semantic structure, and their boundary detection exhibit similar properties.

\boxtimes : Corresponding author.

Therefore, a natural question arises *whether we can address these different kinds of generic boundary detection in a general and unified architecture*. Previous methods [8, 29, 34] mainly focus on building informative feature representations carefully designed for the specific boundary type and cast the boundary detection problem as a dense prediction task. To produce the final boundary detection, they often resort to sophisticated post-processing techniques to remove duplicate false positives. The complicated design and post-processing are highly correlated with specific boundary type and prevent them from generalizing well to different types of generic boundary detection.

To this end, in this paper, we unify the detection of different kinds of boundaries as a temporal sparse detection in long-form videos. We introduce the *Temporal Perceiver*, a general framework designed to handle arbitrary kinds of boundaries using a single Transformer-based architecture. Attention modules are flexible architectural building blocks, but also require computational cost quadratically with the input dimension. Based on the observation that there exists high redundancy among frames within each segment, we argue that it is unnecessary to apply the attention operation in the original temporal resolution of long-form videos.

Our core contribution is to introduce a small set of latent units as anchors to compress the long video sequence into a fixed dimension. These latent units form a cross-attention block to squeeze the input into a latent feature space with fixed and reduced dimension. This step overcomes the unnecessary computation due to temporal redundancy and reduces the computational cost to linear complexity of temporal duration. In particular, videos can be viewed as a series of semantically coherent segments divided by generic boundaries. To effectively capture this temporal structure, we construct the latent units explicitly with boundary queries and context queries. The boundary queries aim to aggregate the important semantic incoherence regions across boundaries, while the context queries are learned to cluster the coherence regions into a few centers. In addition, to avoid the attention training collapse to identical representation for all positions, we propose a new alignment loss to guide the training of cross-attention maps and make this compression process more informative. Finally, we place a transformer decoder on top to perform sparse detection of generic boundaries with a set of learnable proposals. Due to the nature of sparse detection and strict matching criteria during training, our method is free of complicated post-processing and can be generalized to different types of generic boundary detection.

In summary, the contributions are three-fold:

- In this paper, we present *Temporal Perceiver*, a general architecture to tackle generic boundary detection in long-form videos, providing a unified solution to the detection of the arbitrary boundary with Transformers.

- To tackle the temporal redundancy of long videos and reduce the model complexity, we introduce a small set of latent queries for feature compression via cross-attention mechanism, with specific latent query construction to capture the temporal structure of videos and an alignment loss to aid cross-attention training.
- Experiments demonstrate that our method outperforms the existing state-of-the-art methods on shot-level, event-level, and scene-level generic boundary benchmarks.

2. Related Work

Generic Boundary Detection. Generic boundary detection is termed for unified detection of arbitrary temporal generic boundaries. Different boundaries require different levels of visual understanding. Shot boundary in SoccerNet depends on low-level appearance. Event boundary in GEBD is based on motion semantics. Scene boundary in MovieNet is determined by holistic scene understanding.

Previous literature used specific hand-crafted techniques to solve different types of boundaries. Methods from Scikit [12] and PySceneDetect [6] libraries achieved superior performance in shot boundary detection based on frame variations in color or intensity. Previous GEBD methods [14, 19, 22, 24, 25, 33, 34] focused on building representations specifically designed for event-level boundaries and exploited dense prediction paradigm with post-processing. Temporal Convolution Network (TCN) [22, 25] used a two-layer temporal convolution network to densely predict the confidence score for each frame. PC [34] explored the local temporal dependency by generating past and feature features for each temporal location for the final dense confidence estimation. These methods used CNN in a local temporal window to address event boundary and depended heavily on post-processing to remove duplicates. Scene segmentation attracts academic attention from both supervised [3, 26, 29, 31] and unsupervised [7, 8, 17, 30, 32, 36] research. The pioneering method LGSS [29] resorted to LSTM to capture long-range temporal context for scene boundary detection and manually designed a dynamic programming algorithm for post-processing. No previous work has addressed these boundaries in a single and unified framework. In contrast, our temporal perceiver presents a general solution with global view to handle these different types of boundaries without any specific design.

Visual Transformers. Inspired by the great advances of Transformer architecture in NLP field [13, 39], researchers explored the application of such architecture in visual tasks [1, 4, 15, 27, 28, 35, 38]. DETR [4] was the first to successfully utilize a Transformer encoder-decoder structure in object detection task and achieves on par performance with its highly optimized CNN-based counterparts.

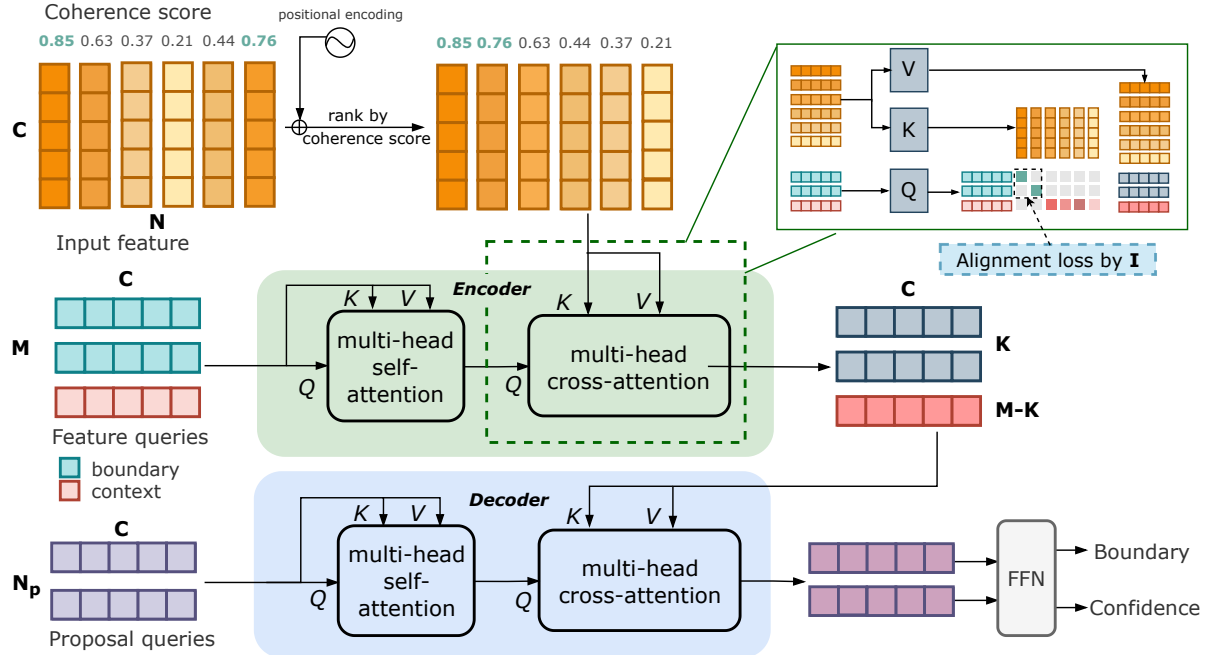


Figure 2. **Pipeline of Temporal Perceiver.** Our model is a general architecture for generic boundary detection. It is composed of a Transformer decoder repurposed as encoder and a Transformer decoder as decoder. The cross-attention layer in encoder takes in large input as key and value. Feature queries are introduced as query to the cross-attention and distills boundary and context information from input. The decoder includes self-attention and cross-attention layers in alternation. Proposal queries aggregate boundary representations from the refined sequence via decoder layers and decoded by FFN head for final predictions.

Despite its success, DETR suffered from the quadratic memory complexity in encoder self-attention layers and therefore had limitations with large input sequences. Deformable DETR [46] replaced the global and dense self-attention in encoder with a set of sparsely sampled reference points and deformable attention mechanism. PnP-DETR [42] performed differentiable sparse sampling on input sequences and reduced the input length to Transformer encoder. RTD [35] extended the idea of DETR to the video domain for temporal action localization with several important improvements. In our approach, we re-purpose the Transformer decoder as an encoder for feature compression in video domain. This decoder-as-encoder structure squeezes temporal redundant input into a small set of feature queries, resulting in a memory-efficient encoder.

Recently, Jaegle *et al.* proposed the Perceiver architecture [21], which handles large inputs through cross-attention to distill inputs into latent arrays and generate informative representations for classification. We developed our method independently, and lately found ourselves to think in-sync with Perceiver. However, our approach aims to tackle concrete tasks with encoder-decoder structure that is capable to generate circumscribed detection results other than just classification logits.

3. Method

3.1. Overview

We propose Temporal Perceiver based on attention layers and Transformers, to efficiently and sparsely locate generic boundaries in long-form videos. Given an untrimmed video X , Temporal Perceiver generates a set of generic boundary proposals $\Psi = \{t_n\}_{n=1}^{N_g}$ to locate the generic boundaries $\hat{\Psi} = \{\hat{t}_n\}_{n=1}^{N_g}$ in video X , with N_g denotes the number of boundary groundtruths.

The main structure of Temporal Perceiver is depicted in Figure 2. We take the frame-level **RGB features** $F \in \mathbb{R}^{N \times C}$ and **coherence scores** $S \in \mathbb{R}^{N \times 1}$ from backbone network as input, where N is the frame number and C is feature dimension. A cross-attention based *encoder* \mathbb{E} and a set of learnable **feature queries** (latent units) $Q_e \in \mathbb{R}^{M \times C}$, distill the input sequence into a latent feature space of reduced dimension $\hat{F} \in \mathbb{R}^{M \times C}$, where M is the number of latent units. The latent unit number is smaller than the original temporal dimension and each unit acts as an anchor to cluster the temporal information in a global view. Based on this compressed representation, we use another Transformer *decoder* \mathbb{D} and a set of learnable **proposal queries** $Q_d \in \mathbb{R}^{N_p \times C}$ to directly and sparsely produce generic boundary representations. Finally, feed forward networks (FFNs) are used as localization head and scoring head to

give the final predictions. Our Temporal Perceiver yields a simple and general temporal structure modeling framework without any post-processing technique, which makes no specific assumption about the boundary type and can be generalized to detect arbitrary generic boundaries.

3.2. Feature Encoding and Coherence Score

We adopt ResNet50 [18] pre-trained on ImageNet [11] as backbone to extract appearance features $F = \{f_i\}_{i=1}^N$ and coherence scores $S = \{s_i\}_{i=1}^N$ from RGB frames. Specifically, we first densely sample snippets from videos. Each snippet contains k frames and is sampled at stride τ . Given a snippet i , we concatenate its k feature vectors encoded by backbone, and then perform temporal convolution, max-pooling and fully-connected layer upon the feature vectors. The output feature f_i is extracted after max-pooling layer. The final fully-connected layer outputs a classification score s_i to represent the probability that its center frame i is boundary. This classification score is the coherence score used in Temporal Perceiver. The backbone network is trained with the dense boundary groundtruth on the benchmarks.

3.3. Temporal Perceiver

The Temporal Perceiver architecture is formulated as an encoder-decoder framework and built upon the Transformers. The encoder, which is a re-purposed Transformer decoder, takes in a set of feature queries and compresses the video feature into a reduced sequence of latent representations. The decoder, which is a vanilla Transformer decoder, directly output final predictions with a set of proposal queries from the compressed feature. The input features of length N are down-scaled into fixed length M via the cross-attention operations in encoder ($M < N$). Compared with the original Transformer encoder, our Temporal Perceiver complexity is reduced from $O(N^2)$ to $O(NM + M^2)$, resulting in linear complexity with a relatively small M .

Encoder: Temporal Compression via Feature Queries. Videos can be divided into two kinds of regions in time, namely boundary regions and context regions (i.e., within each segment). Boundary region refers to the temporal interval around the generic boundary with gradual temporal transition, while context region refers to more central regions within segments. For better localization performance, our main focus is on boundary regions. Context regions are less important and could be compressed into shorter sequences for efficiency. To this end, we build two types of feature queries (boundary queries and context queries) to attend on semantic coherence and incoherence regions accordingly.

Specifically, we distinguish the boundary region and the context region based on dense coherence scores S obtained from backbone. These coherence scores are estimates of

the likelihood that the corresponding location is a generic boundary. We sort the input features according to the descending order of coherence scores and obtain the sorted permutation π . The top K locations with highest coherence scores are taken as boundary regions

$$F_b = \{f_{\pi_n} | n = 1, \dots, K\}. \quad (1)$$

The rest as context regions $F_c = F \setminus F_b$. We allocate M latent feature queries to K boundary queries Q_b and $M - K$ context queries Q_c . These latent queries $Q_e = [Q_b, Q_c]$ are learnable embeddings shared among all videos in the dataset. They are randomly initialized and trained jointly with network weights. Self-attention in encoder models the global dependency for feature queries, adding pair-wise feature interactions throughout the compression. Through cross-attention layers, K boundary queries Q_b handle the features of boundary regions in a one-on-one manner, and $M - K$ context queries Q_c flexibly cluster the vast context regions into a few contextual centers. The overall encoder of Temporal Perceiver is as follows:

$$\begin{aligned} \text{Encoder } \mathbb{E} : \hat{F} = \\ \text{Cross_attention}([F_b, F_c], \text{Self_attention}(Q_e)), \end{aligned} \quad (2)$$

where $\hat{F} \in \mathbb{R}^{M \times C}$ is the compressed video representation for subsequent sparse detection in decoder. The ratio of boundary query to context query is defined by the balance ratio $\beta = \frac{K}{M-K}$.

Alignment Constraint on Cross-attention. To guide the boundary feature queries to attend the actual video boundaries, we incorporate alignment constraint on its cross-attention maps. As we have re-organized the feature sequence according to its coherence score in the ranking step (in Eq. (1)), we could simply introduce an identity matrix based alignment loss on the last cross-attention map of boundary queries. In this sense, each boundary query is enforced to only attend one of top K locations with highest coherence score. For context queries, we allow them to flexibly attend context information without any constraints. With this new training strategy, we find our feature queries can generate more stable compressed feature representations corresponding to both boundaries and context.

Decoder: Sparse Detection via Proposal Queries. We follow the direct proposal generation pipeline in [4, 35] to generate boundary prediction with Transformer decoders and a set of learnable proposal queries. Throughout the stacked self-attention layers and cross-attention layers, the pair-wise dependencies are modeled for proposals via self-attention to avoid duplicates, and the full sequence of reduced features are attended to via cross-attention to generate boundary embedding. Specifically, the sparse detection

is defined as follows:

Decoder \mathbb{D} : $\Phi =$

$$\text{Cross_attention}(\hat{F}, \text{Self_attention}(Q_d)), \quad (3)$$

where $\Phi \in \mathbb{R}^{N_p \times C}$ is the decoded representations for all proposal queries.

The final predictions are decoded from proposal query embedding via a two-branch head architecture. The localization head uses a three-layer MLP to predict the boundary location, and the classification head uses a fully-connected layer followed by sigmoid function to get confidence scores that effectively distinguish boundaries.

3.4. Training

First, we divide video features into fixed-length sequences via a sliding-window manner, short videos are zero-padded and long videos are divided into non-overlapping segments. Then, we filter out those windows with no groundtruth for training.

Label Assignment. Following the practice of [4], We assign positive labels to predictions with groundtruths in a strict matching scheme. For video input X , the groundtruth set is denoted $\hat{\Psi} = \{\hat{t}_n\}_{n=1}^{N_g}$ and the prediction set is denoted $\Psi = \{t_n\}_{n=1}^{N_p}$. N_p is assumed to be larger than N_g . The bipartite matcher searches for an optimal one-on-one matching between the two sets. The matcher minimizes the cost function via hungarian algorithm to seek the optimal matching, then assign positive labels to those predictions that are matched with groundtruths. The cost function is defined as:

$$C = \sum_{n:\sigma(n) \neq \emptyset} \alpha_{loc} \cdot |t_n - \hat{t}_{\sigma(n)}| - \alpha_{cls} \cdot p_n, \quad (4)$$

p_n denotes the boundary confidence score on frame n , σ denotes a permutation for predictions to match with the groundtruths. α_{cls} and α_{loc} denote coefficients for classification error and localization error.

Losses. Conventionally, we define a localization loss and a classification loss to supervise the final predictions. The localization loss is formulated with L_1 loss on predicted boundary point t_n and its matched groundtruth $\hat{t}_{\sigma(n)}$:

$$L_{loc} = \frac{\alpha_{loc}}{N_{pos}} \sum_{n:\sigma'(n) \neq \emptyset} L_1(t_n, \hat{t}_{\sigma(n)}). \quad (5)$$

The classification loss is defined with cross-entropy loss:

$$L_{cls} = -\frac{\alpha_{cls}}{N} \sum_{n=1}^N (l_n \log p_n + (1 - l_n) \log(1 - p_n)), \quad (6)$$

l_n denotes the binary groundtruth label for frame n . We use the same set of classification and localization coefficients for matching cost and loss functions.

To enforce additional constraint on feature compression in order to preserve the important boundary information, we add a diagonal alignment loss L_{align} on cross-attention maps:

$$L_{align} = -\alpha_{align} \cdot \log \frac{1}{K} \sum_{m=1}^K \mathbf{A}_{m,m}. \quad (7)$$

M is the number of feature queries; \mathbf{A} denotes the last-layer cross-attention map; α_{align} is the alignment loss coefficient. It is noted that we use auxiliary loss with classification loss and localization loss, but not with the alignment loss.

3.5. Inference

During inference, we directly and sparsely predict boundary locations as well as their confidence scores without the help of post-processing algorithms, such as watershed, dynamic programming or non-maximum suppression.

We use fully-connected layers as localization and classification heads for final predictions. These heads take in the proposal embedding and output boundary location t_n and its corresponding confidence p_n respectively. The generic boundary detection metrics require results in a hard-submission manner, without directly leveraging the confidence estimation performance. As a result, we threshold our predictions based on confidence threshold γ to filter the most confident predictions for submissions.

4. Experiments

4.1. Dataset and Setup

SoccerNet-v2. SoccerNet-v2 [10] is a large-scale soccer video dataset, containing 200 untrimmed soccer broadcast videos annotated with 158,493 shot boundaries for the task of camera shot boundary detection. Specifically, three types of shot transitions are annotated, including abrupt, fading and logo transition. The annotated games are divided into training, validation and testing set of 120, 40 and 40 videos respectively.

Kinetics-GEBD. Kinetics-GEBD [34] is a recently proposed benchmark for GEBD task. The dataset contains 60K videos and is divided into Train, Val and Test set. The Train and Test set each contains 20K videos from Kinetics-400 Train Set, and the Val set contains 20K videos from Kinetics-400 Val Set. We test our model's performance on Kinetics-GEBD Val set.

TAPOS. TAPOS [33] contains 16,294 valid instances from Olympics sport videos. All instances are split into train, validation and test sets, of sizes 13094, 1790, 1763, respectively. We trim the action instances as input video and detect the sub-action boundaries within the action. The benchmark is re-purposed for generic event boundary detection by Shou et al. [34]. Our model is evaluated on the validation set.

MovieNet. MovieNet [20] dataset is a popular benchmark for Scene Segmentation. It contains 42K annotated scene segments from 318 movies, and it is divided into training, validation and testing sets with 190, 64 and 64 movies respectively. We report ablation results on MovieNet validation set.

Implementation details. We adopt ResNet50 [18] for feature extraction, the sampling stride $\tau = 1$ for SoccerNet-v2, $\tau = 3$ for Kinetics-GEBD and TAPOS. Due to copyright, MovieNet only provides three frames from each shot, so the actual temporal strides between frames can be huge. We strategically take all frames into account and set the sampling stride τ to 1, to mitigate large regression errors caused by wide input stride. The local window size k for frame-level feature extraction is 9 for SoccerNet-v2, 10 for Kinetics-GEBD and TAPOS, 12 for MovieNet.

We process input videos via a sliding-window mechanism for all datasets, the window size N for SoccerNet-v2, Kinetics-GEBD and TAPOS is set to 100 and the window size for MovieNet is set to 30. Short videos are zero-padded to window size. We don't overlap windows, so the overlap ratio is 1 for both training and inference. The refined feature length M is set to 32, 60, 60, 15 for SoccerNet-v2, Kinetics-GEBD, TAPOS and MovieNet; the number of boundary queries and context queries is 20 and 12 for SoccerNet-v2, 48 and 12 for Kinetics-GEBD and TAPOS, 10 and 5 for MovieNet.

The loss parameters α_{cls} , α_{loc} and α_{align} are set to 2, 1, 1 respectively. We use AdamW as optimizer. The learning rate is set to 2e-4 and the batch size is 64. The confidence threshold γ for final submissions is set to 0.9 for SoccerNet-v2, Kinetics-GEBD and TAPOS, 0.7 for MovieNet.

4.2. Shot Boundary Detection

Evaluation Metrics. We follow [10] to use mAP metric with tolerance δ of 1 second for evaluation. A predicted boundary is positive if it falls within the given tolerance δ of a ground-truth timestamp.

Comparison with the state of the art. We train Temporal Perceiver on the training set, validate on the validation set to select the best model, then report the results on the testing set. As Table 1 illustrates, Temporal Perceiver outperforms the previous state-of-the-art method by 3.4%, generalizing well to shot-level generic boundary detection. Our model outperforms previous methods on fading transitions with a large margin of 25% and achieves competitive results on abrupt and logo transitions.

4.3. Event Boundary Detection

Evaluation metrics. We use f1 score under different Relative Distance thresholds for quality measurement. Relative Distance is the relative distance between the predicted

Table 1. Comparison with the state-of-the-art on SoccerNet-v2 in terms of mAP(%). The second best for each column is underlined.

Method	Bound. Det.	Transition		
		Abrupt	Fading	Logo
CALF [9]	59.6	59.0	<u>58.0</u>	61.8
Intensity [12]	64.0	74.3	<u>57.2</u>	28.5
Content [6]	62.2	68.2	49.7	35.5
Histogram [12]	<u>78.5</u>	<u>83.2</u>	54.1	<u>82.2</u>
Temporal Perceiver	81.9	<u>82.4</u>	83.0	<u>78.8</u>

and groundtruth boundary timestamps, divided by the duration of the corresponding video. Given a fixed Relative Distance, we use it as threshold to determine whether a boundary prediction is correct, then the f1 metrics can be computed.

Comparison with the state of the art. In Table 2, we compare the results of temporal perceiver with the state-of-the-art methods on Kinetics-GEBD and TAPOS for GEBD and TAP task respectively. The results show that our method comfortably outperforms the state-of-the-art method especially with a lower Rel.Dis. threshold (lower error tolerance). This demonstrates that our model produces more precise and accurate boundary predictions than previous methods.

4.4. Scene Boundary Detection

Evaluation metrics. Following [29], we use Average Precision (AP) and M_{iou} to evaluate the quality of detected scene boundaries, where M_{iou} calculates the weighted sum of intersection-over-union of a detected scene with respect to its distance to the closest ground-truth scene.

Comparison with the state of the art. We quote the results from [29] and continue to report on MovieScenes [29] (a 150-video subset of MovieNet [20]) with 100, 20 and 30 videos for train, validation and testing respectively. However, the exact data-splits are not provided. Thus, we apply a 10-fold cross-validation on the dataset and report the mean and standard deviation of AP and M_{iou} .

In Table 3, we compare the results of Temporal Perceiver with the state-of-the-art methods on MovieScenes. To compute Average Precision, we construct Gaussian distributions centered at our sparsely-predicted locations to approximate dense score sequences for each video. AP is reported based on the approximated dense scores. Results show that our method surpasses the previous methods, demonstrating the generalization ability and effectiveness of our model on generic boundary detection under various granularity.

4.5. Efficiency Analysis

We analyze Temporal Perceiver's advantage in efficiency in terms of Shot Per Second (SPS) in inference and FLOPs of feature encoders on MovieNet. We compare our model

Table 2. Comparison with other state-of-the-art methods on Kinetics-GEBD and TAPOS in terms of f1@Rel.Dis.

Rel.Dis. threshold		0.05	0.1	0.15	0.2	0.25	0.3	0.35	0.4	0.45	0.5	avg	
Kinetics-GEBD		BMN [24]	0.186	0.204	0.213	0.220	0.226	0.230	0.233	0.237	0.239	0.241	0.223
		BMN-StartEnd [24]	0.491	0.589	0.627	0.648	0.660	0.668	0.674	0.678	0.681	0.683	0.640
		TCN-TAPOS [22,25]	0.464	0.560	0.602	0.628	0.645	0.659	0.669	0.676	0.682	0.687	0.627
		TCN [22,25]	0.588	0.657	0.679	0.691	0.698	0.703	0.706	0.708	0.710	0.712	0.685
		PC [34]	0.625	0.758	0.804	0.829	0.844	0.853	0.859	0.864	0.867	0.870	0.817
		Temporal Perceiver	0.751	0.821	0.841	0.852	0.862	0.865	0.867	0.869	0.872	0.877	0.846
TAPOS		TCN [22,25]	0.237	0.312	0.331	0.339	0.342	0.344	0.347	0.348	0.348	0.348	0.330
		TransParser [33]	0.289	0.381	0.435	0.475	0.500	0.514	0.527	0.534	0.540	0.545	0.474
		PC [34]	0.522	0.595	0.628	0.646	0.659	0.665	0.671	0.676	0.679	0.683	0.642
		Temporal Perceiver	0.552	0.663	0.713	0.738	0.757	0.765	0.774	0.779	0.784	0.788	0.732

Table 3. Comparison with the state-of-the-art on MovieNet in terms of AP and M_{iou} .

Method	Modality	AP (\uparrow)	M_{iou} (\uparrow)
GraphCut [30]	Visual	14.1	29.7
SCSA [7]	Visual	14.7	30.5
DP [17]	Visual	15.5	32.0
Grouping [31]	Visual	17.6	33.1
StoryGraph [36]	Visual	25.1	35.7
Siamese [3]	Visual	28.1	36.0
LGSS [29]	Visual	47.1	48.8
Temporal Perceiver	Actor Action	50.4 ± 1.6	52.0 ± 1.2
Temporal Perceiver*	Visual	51.2	52.5

* results are reported on MovieNet.

Table 4. Efficiency analysis with previous method on MovieNet.

Method	ShotPS(\uparrow)	GFLOPs (\downarrow)
LGSS [29]	60.7	8141
Transformers	371.1	66
Temporal Perceiver	377.9	49

Table 5. Ablation studies on alignment loss on MovieNet and Kinetics-GEBD.

Alignment Loss	MovieNet		Kinetics-GEBD
	AP	M_{iou}	f1@0.05
\times	50.62	51.89	73.60
\checkmark	51.21	52.51	75.12

with the previous state-of-the-art method LGSS and a Transformers baseline method. The results are reported on one RTX 2080-Ti GPU. Input is restricted to three random movies selected from MovieNet validation set and contains 2275 shots in total. Tab. 4 shows that compared to the baseline method, our model is more efficient with 6 more shots processed per second and 0.7 times less FLOPs count, due to effective feature compression. Free of post-processing modules, Temporal Perceiver infers 6 times faster with much less FLOPs than LGSS.

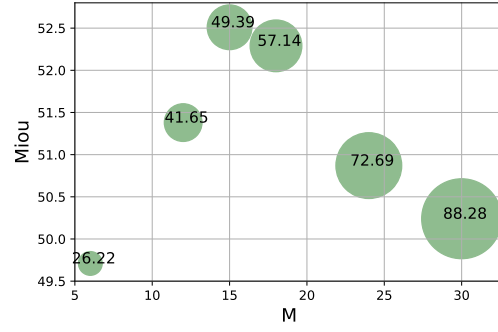


Figure 3. Ablation studies on feature compression on MovieNet.

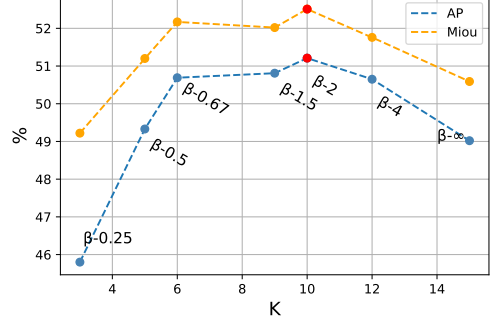


Figure 4. Ablation studies on query construction on MovieNet.

4.6. Ablation Study

Study on feature compression. With latent queries and cross-attention mechanism, we reduce the temporal redundancy and model complexity via feature compression. Figure 3 shows the M_{iou} and encoder FLOPs on MovieNet under different settings of M . The point size and the captions represent encoder GFLOPs. The M_{iou} performance reaches the peak at $M = 15$, indicating $M = 15$ the sweet spot for compression without severe information loss. Interestingly, lower compression also performs worse. We contend that high compression results in loss of important context while at low compression, the video redundancy would distort the quality of compressed features, making $M = 15$ a perfect solution for balance and efficiency. Compared with the



Figure 5. **Visualization of feature compression on MovieNet.** The figure contains four rows, the first and the last row are scene content. The second row is an overview of groundtruths within this video and the third row shows detailed segment groundtruth and coherence confidence.

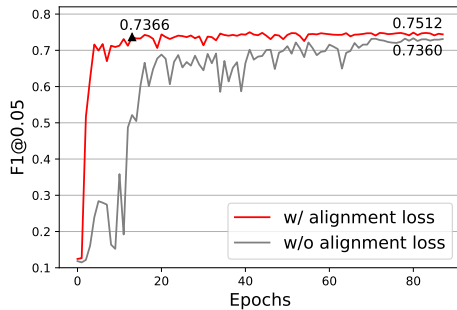


Figure 6. Ablation studies on alignment loss with respect to model convergence.

zero-compression ($M = 30$) setting, our design improves the performance by 2% in M_{iou} and reduces the FLOPs by half.

Study on query construction. With specific latent query construction, we exploit the semantic structure of long-form videos and compress features into stable latent queries. The balance ratio β of boundary and context queries in feature construction needs consideration. Various β are tested under a fixed $M = 15$. Figure 4 shows that the detection performance is sub-optimal at both ends of the curve. The performance drops drastically at extremely small β . We argue that when there are few boundary queries (small β), the compressed features lack discriminative boundary information, explaining the weak performance. The performance is also weak at $\beta \rightarrow \infty$ without context queries, demonstrating the complementary contributions of context information. We report with the setting $\beta = 2$ for the best performance, indicating that boundary information benefits the detection performance more than context information.

Study on alignment loss. The alignment loss is proposed to help the cross-attention learning and prevent feature col-



Figure 7. Visualization of qualitative results on MovieNet.

lapse at early stage. Table 5 reports the ablation results on the alignment loss. With the additional alignment supervision, the $f1@0.05$ performance increases by 1.5% on Kinetics-GEBD benchmark, and the M_{iou} and AP performance increases by 0.7% and 0.6% on MovieNet. In addition, we plot the convergence curve on Kinetics-GEBD in Figure 6, the results show that the model converges nearly 7 \times faster with the alignment loss, and has a 2% performance gain under $f1@0.05$ metric.

5. Visualization

Visualization of feature compression. We perform feature compression on boundary and context regions and distinguish these regions based on the coherence estimation scores. Fig. 5 shows an example of feature compression with MovieNet video segment. The scores are visualized in row 3. The darker color represents a bigger likeliness of frames to cover incoherence regions. In the visualization of video content and groundtruth, we observe temporal redundancy in scene 6. Meanwhile, the darker units are observed

to cluster near groundtruth boundaries, but not in the region within scene 6. As a result, the redundant frames in scene 6 are not marked as boundaries and would be clustered into few contextual centers, fulfilling redundancy compression. **Visualization of qualitative results.** We provide the qualitative results on a randomly selected segment from the validation set of MovieNet. In Fig. 7, we visualize the groundtruth boundaries and the predictions from our model and previous SOTA method LGSS in row 1, 3 and 2. The LGSS results are reproduced on MovieNet with multi-modal input. Compared with LGSS results, our method does not produce duplicates around groundtruth or other within-scene false positives and is able to detect the generic boundary with accurate localization.

6. Conclusion

In this paper, we have presented Temporal Perceiver, a general architecture for generic boundary detection. It offers an efficient and effective pipeline with Transformer architecture and provides a unified framework for sparse detection of arbitrary generic boundaries. The core contribution is to utilize cross-attention blocks to squeeze redundant video input into a fixed dimension, with a small group of latent units as anchors, which mitigates the issue of temporal redundancy in long-form videos and reduces model complexity to linear-level. Moreover, we construct the latent units with boundary and context queries to pattern cross-boundary incoherence and within-context coherence respectively. Furthermore, to avoid feature collapse, we introduce a new alignment loss for feature-query alignment. Finally, the sparse detection paradigm of transformer decoder allows our model to be free of post-processing, thus generalizing well to different generic boundary detection. Experiments show that Temporal Perceiver achieves state-of-the-art results on benchmarks of shot-level, event-level, and scene-level generic boundaries.

A. Further Ablation Study

In this section, we conduct extensive ablation experiments on the alignment loss, which are left out in the main paper due to space limitation. In addition, we also report ablation studies on Kinetics-GEBD to demonstrate the generalization ability of Temporal Perceiver.

A.1. Study on alignment loss

In order to build stable boundary-context representations, the boundary queries attend to boundary features in a one-on-one manner via alignment supervision on the last layer of encoder cross-attention. For the design simplicity, one may ask: *why not directly use boundary features instead of boundary queries?* In Table A, We compare the results of the alignment loss guided model and another variant model that discards the boundary queries and directly concatenates the boundary features with learned context centers. On both benchmarks, the performance of the direct concatenation variant is weaker than the alignment loss-guided model. We contend that boundary queries encode vital prior in these shared weights, and layers of self-attention operation model the pair-wise interaction among the queries, expanding the receptive field for each boundary query.

Table A. Ablation studies on alignment loss on MovieNet and Kinetics-GEBD.

Variants	MovieNet		Kinetics-GEBD
	AP (%)	M_{iou} (%)	f1@0.05(%)
Direct Concatenation	49.62	52.17	73.46
Alignment Loss	51.21	52.51	75.12

A.2. Study on feature compression

To further study feature compression on videos with different types of generic boundaries, we conduct extensive experiments on Kinetics-GEBD benchmark under compression ratios $\frac{M}{N}$, ranging from 0.2 to 1 of stride 0.2. Figure A shows that when $M = 0.6N$, the model achieves the best performance. As the compression ratio decreases from 0.6 to 0.4, the f1 performance drops slightly by 0.23%. When the compression ratio is 0.2, the f1 performance drops drastically with a decrease of 1.14%. We infer that the lower bound for compression is 0.4 for Kinetics-GEBD dataset and set the compression ratio as 0.6 for the best performance.

A.3. Study on query construction

We study the boundary-context query balance on Kinetics-GEBD to see if it shares the same pattern as on MovieNet. In Figure B, the f1 performance is plotted under

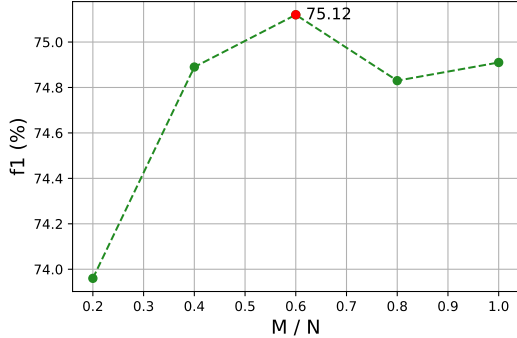


Figure A. Ablation studies on feature compression on Kinetics-GEBD.

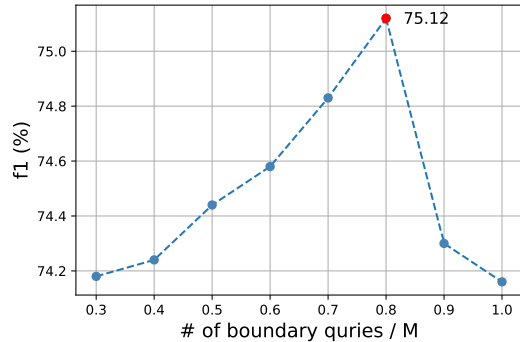


Figure B. Ablation studies on query construction on Kinetics-GEBD.

different proportion of boundary queries with a fixed compression capacity $M = 0.6N$. We evaluate the model under boundary query proportions ranging from 0.3 to 1.0 with a stride of 0.1. The model achieves the best performance when the number of boundary queries equals to $0.8M$, which conveys the same message as with MovieNet, that the boundary information is more beneficial than context information to boundary detection. The performance decrease with few boundary queries or context queries is more obvious on Kinetics-GEBD. When the number of boundary queries equals to $0.3M$, the performance drops by nearly 1% from the best; and when the proportion equals to 1 with zero context queries, the performance drops by 1%, indicating the complementary contributions of context queries.

B. Visualization

In this section, we provide visualization of encoder cross-attention and self-attention layers to unveil the detailed pattern for compression. In addition, we visualize the qualitative results and feature compression on Kinetics-GEBD to prove the effectiveness and generalization ability of Temporal Perceiver.

B.1. Encoder cross-attention

Figure C is the visualization of cross-attention blocks in all 6 layers of encoder on a randomly selected video of Kinetics-GEBD. In the first 2 layers, the latent queries aggregate information from both the boundary and context regions as an initialization. In the third to fifth layer, latent queries attend to parts of boundary regions and context regions. The beam patterns appear at different parts for each layer without overlap. In the last layer, guided by the diagonal alignment loss, most of the boundary queries aggregate corresponding boundary features in a diagonal-alike pattern, with a few out-of-line attention on neighboring features. The context queries are free of additional supervision and still learn to cluster the contextual centers within the context region.

B.2. Encoder self-attention

Figure D is the visualization of self-attention blocks in all 6 layers of encoder on a randomly selected video of Kinetics-GEBD. In the first three layers, the latent queries exchange information from all queries. In the last three layers, all latent queries have similar attention peaks on certain latent queries. These latent queries are mostly boundary queries. It is also observed that the pair-wise interactions between boundary query and context query is established in all layers.

B.3. Feature compression on Kinetics-GEBD

The feature compression process is illustrated in Figure E. The input video is about doing laundry, it is randomly selected from Kinetics-GEBD validation set. We observe that similar to the visualization on MovieNet, the coherence prior gives a coarse yet reliable estimation of boundary regions. Row 4 visualizes the top- K boundary regions in dark color. All groundtruths are covered in boundary regions. Meanwhile, the temporal redundancy between generic boundaries, such as the repeated back-and-forth movement of pouring detergent in the fourth segment, are excluded and would be clustered in a few centers.

B.4. Qualitative results on Kinetics-GEBD

We visualize the qualitative results in Figure F. The results are reported on a video of shredding papers. Compared to the previous state-of-the-art method PC, the predictions of Temporal Perceiver are more accurate, with less relative distance to groundtruth and fewer false positives due to the relatively intense within-event motion in the third segment.

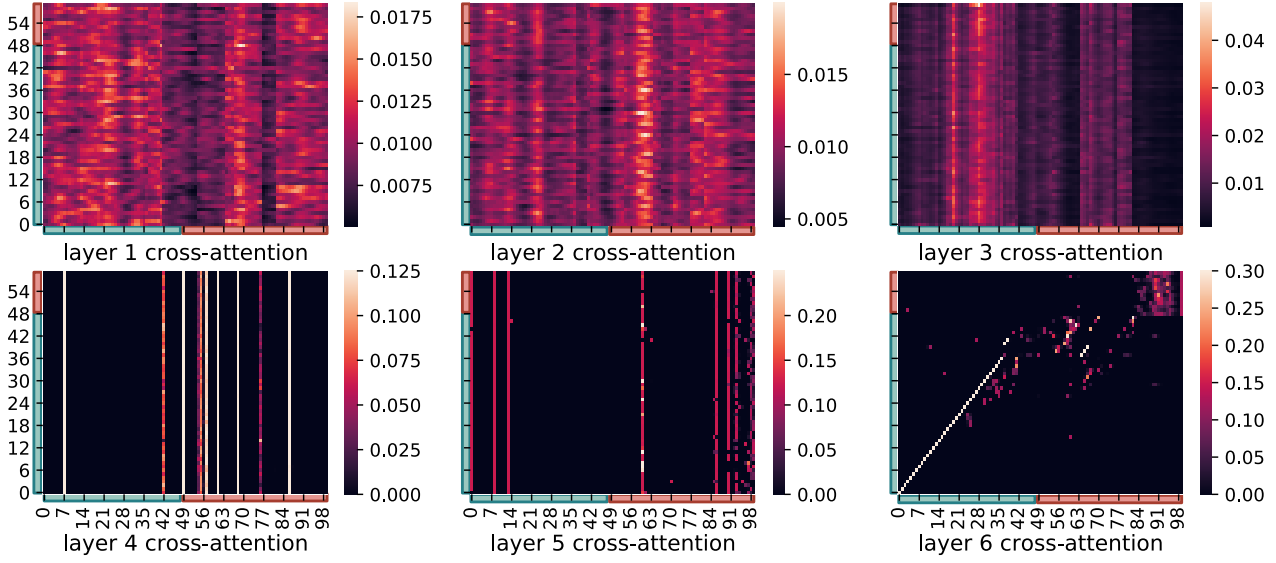


Figure C. **Visualization of encoder cross-attention layers.** The x-axis is the temporal locations in input sequence, and the y-axis is the temporal locations of latent queries. Boundary queries and features are covered in green, while context queries and features are covered in red.

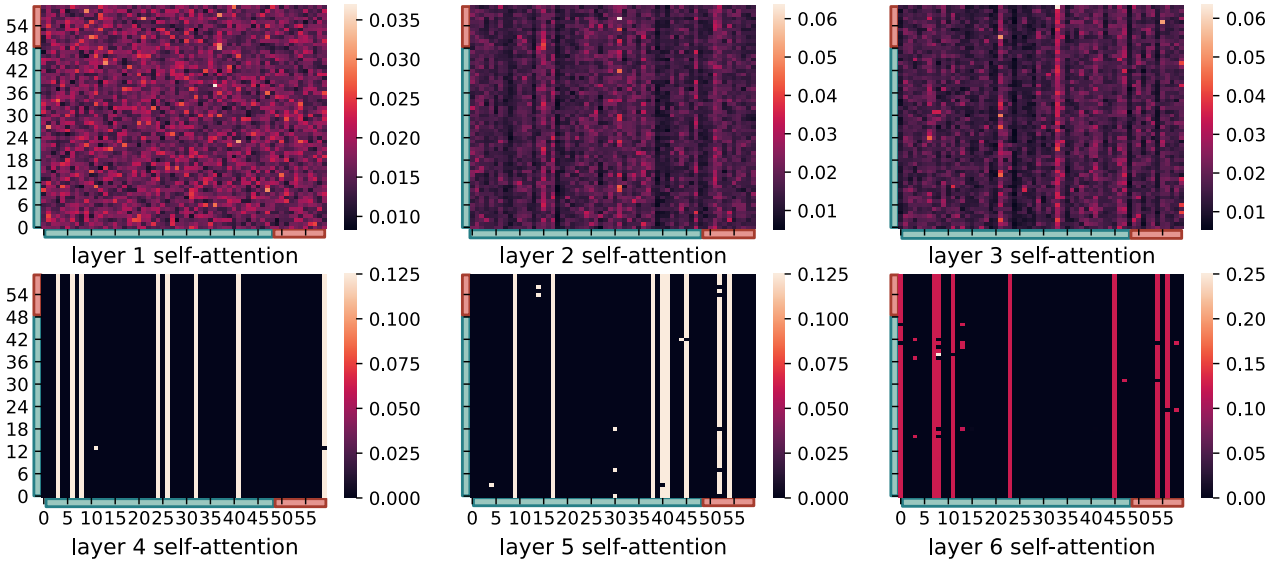


Figure D. **Visualization of encoder self-attention layers.** The x-axis and the y-axis are the temporal locations of latent queries. The x-axis represents input and the y-axis represents output. Boundary queries are covered in green, while context queries are covered in red.

References

- [1] Anurag Arnab, Mostafa Dehghani, Georg Heigold, Chen Sun, Mario Lučić, and Cordelia Schmid. Vivit: A video vision transformer. In *ICCV*, pages 6836–6846. IEEE, October 2021. [2](#)
- [2] Yueran Bai, Yingying Wang, Yunhai Tong, Yang Yang, Qiyue Liu, and Junhui Liu. Boundary content graph neural network for temporal action proposal generation. In *ECCV* (28), volume 12373 of *Lecture Notes in Computer Science*, pages 121–137. Springer, 2020. [1](#)
- [3] Lorenzo Baraldi, Costantino Grana, and Rita Cucchiara. A deep siamese network for scene detection in broadcast videos. In *ACM Multimedia*, pages 1199–1202, 2015. [2](#), [7](#)
- [4] Nicolas Carion, Francisco Massa, Gabriel Synnaeve, Nicolas Usunier, Alexander Kirillov, and Sergey Zagoruyko. End-to-

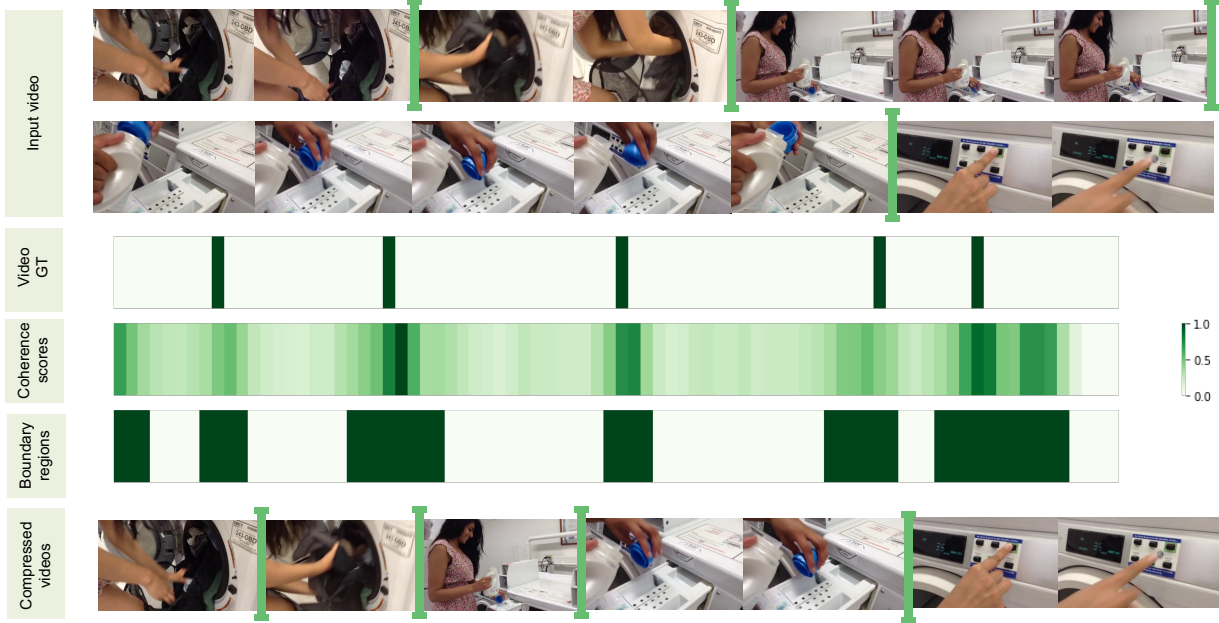


Figure E. Visualization of feature compression on Kinetics-GEBD.



Figure F. Visualization of qualitative results on Kinetics-GEBD.

end object detection with transformers. In *ECCV(1)*, volume 12346 of *Lecture Notes in Computer Science*, pages 213–229. Springer, 2020. 2, 4, 5

[5] João Carreira and Andrew Zisserman. Quo vadis, action recognition? A new model and the kinetics dataset. In *CVPR*, pages 4724–4733. IEEE Computer Society, 2017. 1

[6] Brandon Castellano. Pyscenedetect: Video scene cut detection and analysis tool. <https://github.com/Breakthrough/PySceneDetect>, 2014. 2, 6

[7] Vasileios Chasanis, Aristidis Likas, and Nikolas P. Galatsanos. Scene detection in videos using shot clustering and sequence alignment. *IEEE Trans. Multim.*, 11(1):89–100, 2009. 2, 7

[8] Shixing Chen, Xiaohan Nie, David Fan, Dongqing Zhang, Vimal Bhat, and Raffay Hamid. Shot contrastive self-supervised learning for scene boundary detection. In *CVPR*, pages 9796–9805, 2021. 2

[9] Anthony Cioppa, Adrien Deliège, Silvio Giancola, Bernard Ghanem, Marc Van Droogenbroeck, Rikke Gade, and Thomas B. Moeslund. A context-aware loss function for action spotting in soccer videos. In *CVPR*, pages 13123–13133. Computer Vision Foundation / IEEE, 2020. 6

[10] Adrien Deliège, Anthony Cioppa, Silvio Giancola, Meisam Jamshidi Seikavandi, Jacob V. Dueholm, Kamal Nasrollahi, Bernard Ghanem, Thomas B. Moeslund, and Marc Van Droogenbroeck. Soccernet-v2: A dataset and benchmarks for holistic understanding of broadcast soccer videos. In *CVPR Workshops*, pages 4508–4519. Computer Vision Foundation / IEEE, 2021. 1, 5, 6

[11] Jia Deng, Wei Dong, Richard Socher, Li-Jia Li, Kai Li, and Li Fei-Fei. Imagenet: A large-scale hierarchical image database. In *CVPR*, pages 248–255. IEEE Computer Society, 2009. 4

[12] Scikit-Video Developers. Scikit-video: Video processing in

python,. <https://github.com/scikit-video/scikit-video.>, 2015. 2, 6

[13] Jacob Devlin, Ming-Wei Chang, Kenton Lee, and Kristina Toutanova. BERT: pre-training of deep bidirectional transformers for language understanding. In *NAACL-HLT*, pages 4171–4186, 2019. 2

[14] Li Ding and Chenliang Xu. Weakly-supervised action segmentation with iterative soft boundary assignment. In *CVPR*, pages 6508–6516. Computer Vision Foundation / IEEE Computer Society, 2018. 2

[15] Alexey Dosovitskiy, Lucas Beyer, Alexander Kolesnikov, Dirk Weissenborn, Xiaohua Zhai, Thomas Unterthiner, Mostafa Dehghani, Matthias Minderer, Georg Heigold, Sylvain Gelly, Jakob Uszkoreit, and Neil Houlsby. An image is worth 16x16 words: Transformers for image recognition at scale. In *ICLR*, 2021. 2

[16] Jialin Gao, Zhixiang Shi, Guanshuo Wang, Jian Li, Yufeng Yuan, Shiming Ge, and Xi Zhou. Accurate temporal action proposal generation with relation-aware pyramid network. In *AAAI*, pages 10810–10817. AAAI Press, 2020. 1

[17] Bo Han and Weiguo Wu. Video scene segmentation using a novel boundary evaluation criterion and dynamic programming. In *ICME*, pages 1–6, 2011. 2, 7

[18] Kaiming He, Xiangyu Zhang, Shaoqing Ren, and Jian Sun. Deep residual learning for image recognition. In *CVPR*, pages 770–778. IEEE Computer Society, 2016. 4, 6

[19] De-An Huang, Li Fei-Fei, and Juan Carlos Niebles. Connectionist temporal modeling for weakly supervised action labeling. In *ECCV*, pages 137–153, 2016. 2

[20] Qingqiu Huang, Yu Xiong, Anyi Rao, Jiaze Wang, and Dahua Lin. Movienet: A holistic dataset for movie understanding. In *ECCV*, pages 709–727, 2020. 1, 6

[21] Andrew Jaegle, Felix Gimeno, Andy Brock, Oriol Vinyals, Andrew Zisserman, and João Carreira. Perceiver: General perception with iterative attention. In *ICML*, pages 4651–4664, 2021. 3

[22] Colin Lea, Austin Reiter, René Vidal, and Gregory D. Hager. Segmental spatiotemporal cnns for fine-grained action segmentation. In *ECCV (3)*, volume 9907 of *Lecture Notes in Computer Science*, pages 36–52. Springer, 2016. 2, 7

[23] Yixuan Li, Zixu Wang, Limin Wang, and Gangshan Wu. Actions as moving points. In *ECCV (16)*, volume 12361 of *Lecture Notes in Computer Science*, pages 68–84. Springer, 2020. 1

[24] Tianwei Lin, Xiao Liu, Xin Li, Errui Ding, and Shilei Wen. BMN: boundary-matching network for temporal action proposal generation. In *ICCV*, pages 3888–3897, 2019. 1, 2, 7

[25] Tianwei Lin, Xu Zhao, Haisheng Su, Chongjing Wang, and Ming Yang. BSN: boundary sensitive network for temporal action proposal generation. In *ECCV (4)*, volume 11208 of *Lecture Notes in Computer Science*, pages 3–21. Springer, 2018. 2, 7

[26] Dong Liu, Nagendra Kamath, Subhabrata Bhattacharya, and Rohit Puri. Adaptive context reading network for movie scene detection. *IEEE Trans. Circuits Syst. Video Technol.*, 31(9):3559–3574, 2021. 2

[27] Ze Liu, Yutong Lin, Yue Cao, Han Hu, Yixuan Wei, Zheng Zhang, Stephen Lin, and Baining Guo. Swin transformer: Hierarchical vision transformer using shifted windows. In *ICCV*, pages 10012–10022, 2021. 2

[28] Ze Liu, Jia Ning, Yue Cao, Yixuan Wei, Zheng Zhang, Stephen Lin, and Han Hu. Video swin transformer. *CoRR*, abs/2106.13230, 2021. 2

[29] Anyi Rao, Linning Xu, Yu Xiong, Guodong Xu, Qingqiu Huang, Bolei Zhou, and Dahua Lin. A local-to-global approach to multi-modal movie scene segmentation. In *CVPR*, pages 10143–10152, 2020. 2, 6, 7

[30] Zeeshan Rasheed and Mubarak Shah. Scene detection in hollywood movies and TV shows. In *CVPR (2)*, pages 343–350. IEEE Computer Society, 2003. 2, 7

[31] Daniel Rotman, Dror Porat, and Gal Ashour. Robust and efficient video scene detection using optimal sequential grouping. In *ISM*, pages 275–280, 2016. 2, 7

[32] Yong Rui, Thomas S. Huang, and Sharad Mehrotra. Exploring video structure beyond the shots. In *ICMCS*, pages 237–240. IEEE Computer Society, 1998. 2

[33] Dian Shao, Yue Zhao, Bo Dai, and Dahua Lin. Intra- and inter-action understanding via temporal action parsing. In *CVPR*, pages 727–736, 2020. 2, 5, 7

[34] Mike Zheng Shou, Stan Weixian Lei, Weiyao Wang, Deepti Ghadiyaram, and Matt Feiszli. Generic event boundary detection: A benchmark for event segmentation. In *ICCV*, pages 8075–8084, 2021. 1, 2, 5, 7

[35] Jing Tan, Jiaqi Tang, Limin Wang, and Gangshan Wu. Relaxed transformer decoders for direct action proposal generation. In *ICCV*, pages 13526–13535, 2021. 2, 3, 4

[36] Makarand Tapaswi, Martin Bäuml, and Rainer Stiefelhagen. Storygraphs: Visualizing character interactions as a timeline. In *CVPR*, pages 827–834, 2014. 2, 7

[37] Yao Teng, Limin Wang, Zhifeng Li, and Gangshan Wu. Target adaptive context aggregation for video scene graph generation. In *ICCV*, pages 13688–13697. IEEE, October 2021. 1

[38] Hugo Touvron, Matthieu Cord, Matthijs Douze, Francisco Massa, Alexandre Sablayrolles, and Hervé Jégou. Training data-efficient image transformers & distillation through attention. In *ICML*, volume 139 of *Proceedings of Machine Learning Research*, pages 10347–10357. PMLR, 2021. 2

[39] Ashish Vaswani, Noam Shazeer, Niki Parmar, Jakob Uszkoreit, Llion Jones, Aidan N. Gomez, Łukasz Kaiser, and Illia Polosukhin. Attention is all you need. In *NIPS*, pages 5998–6008, 2017. 2

[40] Limin Wang, Zhan Tong, Bin Ji, and Gangshan Wu. TDN: temporal difference networks for efficient action recognition. In *CVPR*, pages 1895–1904. Computer Vision Foundation / IEEE, 2021. 1

[41] Limin Wang, Yuanjun Xiong, Zhe Wang, Yu Qiao, Dahua Lin, Xiaoou Tang, and Luc Van Gool. Temporal segment networks: Towards good practices for deep action recognition. In *ECCV (8)*, volume 9912 of *Lecture Notes in Computer Science*, pages 20–36. Springer, 2016. 1

[42] Tao Wang, Li Yuan, Yunpeng Chen, Jiashi Feng, and Shuicheng Yan. Pnp-detr: Towards efficient visual analy-

sis with transformers. In *ICCV*, pages 4661–4670. IEEE, October 2021. 3

[43] Zhenzhi Wang, Ziteng Gao, Limin Wang, Zhifeng Li, and Gangshan Wu. Boundary-aware cascade networks for temporal action segmentation. In *ECCV*, pages 34–51, 2020. 1

[44] Mengmeng Xu, Chen Zhao, David S. Rojas, Ali K. Thabet, and Bernard Ghanem. G-TAD: sub-graph localization for temporal action detection. In *CVPR*, pages 10153–10162. Computer Vision Foundation / IEEE, 2020. 1

[45] Yuan Zhi, Zhan Tong, Limin Wang, and Gangshan Wu. Mgsampler: An explainable sampling strategy for video action recognition. In *ICCV*, pages 1513–1522. IEEE, October 2021. 1

[46] Xizhou Zhu, Weijie Su, Lewei Lu, Bin Li, Xiaogang Wang, and Jifeng Dai. Deformable DETR: deformable transformers for end-to-end object detection. In *ICLR*, 2021. 3